



CHEMISTRY & SUSTAINABILITY

# CHEM **SUS** CHEM

ENERGY & MATERIALS

## Accepted Article

**Title:** Tandem hydrogenolysis–hydrogenation of lignin-derived oxygenates over integrated dual catalysts with optimized interoperations

**Authors:** Youzhu Yuan, Huihuang Fang, Weikun Chen, Shuang Li, Xuehui Li, Xinping Duan, and Linmin Ye

This manuscript has been accepted after peer review and appears as an Accepted Article online prior to editing, proofing, and formal publication of the final Version of Record (VoR). This work is currently citable by using the Digital Object Identifier (DOI) given below. The VoR will be published online in Early View as soon as possible and may be different to this Accepted Article as a result of editing. Readers should obtain the VoR from the journal website shown below when it is published to ensure accuracy of information. The authors are responsible for the content of this Accepted Article.

**To be cited as:** *ChemSusChem* 10.1002/cssc.201902029

**Link to VoR:** <http://dx.doi.org/10.1002/cssc.201902029>

WILEY-VCH

[www.chemsuschem.org](http://www.chemsuschem.org)

A Journal of



# Tandem hydrogenolysis–hydrogenation of lignin-derived oxygenates over integrated dual catalysts with optimized interoperations

Huihuang Fang,<sup>[a]</sup> Weikun Chen,<sup>[a]</sup> Shuang Li,<sup>[b]</sup> Xuehui Li,<sup>[c]</sup> Xinping Duan,<sup>[a]</sup> Linmin Ye,<sup>[a]</sup> and Youzhu Yuan<sup>\*[a]</sup>

**Abstract:** The efficient hydrodeoxygenation (HDO) of lignin-derived oxygenates is essential but challenging due to the inherent complexity of feedstock and the lack of effective catalytic approaches. In this study, we present a catalytic strategy that separates C–O hydrogenolysis and aromatic hydrogenation on different active catalysts with interoperation that can achieve high oxygen removal in lignin-derived oxygenates. The flexible use of tungsten carbide for a C–O bond cleavage and Ni catalyst with controlled particle size for arene hydrogenation enables the tunable production of cyclohexane and cyclohexanol with almost guaiacol conversions. Such integration of dual catalysts with closed proximity performs the superior HDO activity of actual bio-oils into liquid alkanes with a high mass and carbon yield of 27.9 and 45.0 wt%, respectively. This finding provides a new effective strategy for practical applications.

## Introduction

The catalytic transformation of lignocellulose into sustainable fuels and chemicals is an important process that exhibits potential in fossil energy substitution.<sup>[1]</sup> Longstanding interest in lignin utilization has been translated into limited commercial availability due to the lack of innovative catalysts and high-yield practical strategies.<sup>[2]</sup> At present, several approaches have been developed for lignin conversion, including hydrolysis, enzymatic treatment, catalytic depolymerization, and thermochemical conversion.<sup>[3]</sup> Among these approaches, rapid pyrolysis is the leading and most cost-effective process for the direct production of ungradable bio-oils from lignocellulose.<sup>[4]</sup> Nevertheless, such bio-oils are far from commercial use in chemical production and transportation fuels because the rapid pyrolysis results in the formation of complex mixtures of oxygenated compounds, including carbonyls, acids, furans, and complex (alkyl)guaiacols, containing high oxygen content with high viscosity, low energy density, and chemical instability.<sup>[5]</sup> The catalytic

hydrodeoxygenation (HDO) process is viable for extensive oxygen removal in the final upgrading of bio-oils and is a key research subject that has attracted tremendous interests in recent years.<sup>[1c,5b,6]</sup> However, the inherent complexity and high oxygen content of bio-oil components pose a challenging task for current hydroprocessing catalysts, which enable the lignin-to-chemical cycle to achieve high-yield performance and cost-effectiveness.

As popular hydrogenation catalysts, supported metallic catalysts are commonly used catalytic materials in typical HDO processes.<sup>[3a,5b,7]</sup> Numerous studies have shown that supported noble metal catalysts (e.g., Pt, Pd, Ru, and Rh) possess promising HDO activity primarily in lignin-derived platform chemicals, such as anisole and guaiacol, with considerable catalyst lifetimes.<sup>[3a,8]</sup> The high cost of noble metals with moderate performance motivates the development of inexpensive metals, such as Ni, Cu, and Fe, in HDO reactions.<sup>[9]</sup> Such metals have been proven to activate H<sub>2</sub>. However, a typical HDO reaction has been realized in a case with a two-step process involving the hydrogenation of unsaturated C=C and C=O bonds and deoxygenation by using a C–O bond cleavage.<sup>[10]</sup> Metal sites alone are incompetent for efficient hydrogenation and deoxygenation and constantly lead to poor HDO performance.

Bifunctional metal-acid catalysts have emerged and display remarkably enhanced HDO activities.<sup>[3c,11–14]</sup> Given that metal sites facilitate the activation of hydrogen, the acidic sites on the supports are crucial for deoxygenation. Zhao et al.<sup>[12]</sup> made impressive progress on designing metal–acid bifunctional sites, such as Ni/SiO<sub>2</sub> and Ni/HZSM-5, for the efficient conversion of phenolic bio-oil into alkanes. Xia et al.<sup>[3c]</sup> used a Pt/NbOPO<sub>4</sub> catalyst for the production of alkanes from raw lignocellulose whose high activity originated from the synergistic effect between Pt, acidic sites, and NbO<sub>x</sub> species. Similarly, Pd/m-MoO<sub>3</sub>–P<sub>2</sub>O<sub>5</sub>/SiO<sub>2</sub> was devoted to the HDO of water-insoluble bio-oils<sup>[11d]</sup>. Recently, Ju et al.<sup>[6b]</sup> used Pt–alumina/zeolite with optimized acid/metal interaction, which can catalyze the HDO of bio-oxygenates into hydrocarbons. In addition, Al<sub>2</sub>O<sub>3</sub>, TiO<sub>2</sub>, ZrO<sub>2</sub>, and zeolites have also been utilized in preparing bifunctional catalysts.<sup>[13]</sup> Nevertheless, the balance between metal–acid sites is unfeasible to regulate, and the excess incorporation of strong acid sites constantly causes cracking, transalkylation, polymerization, coke formation, and other undesirable side reactions.<sup>[14]</sup>

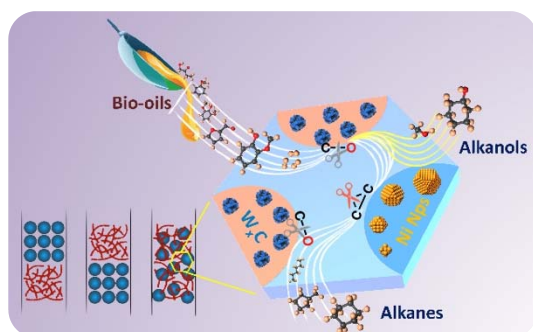
Here, we present an integrated strategy that separates the C–O bond cleavage and aromatic hydrogenation on different active catalysts through a complementary interoperation of dual

[a] H. Fang, W. Chen, Dr. X. Duan, Dr. L. Ye, Prof. Dr. Y. Yuan\*  
State Key Laboratory of Physical Chemistry of Solid Surfaces,  
National Engineering Laboratory for Green Chemical Productions of  
Alcohols-Ethers-Esters and iChEM, College of Chemistry and  
Chemical Engineering, Xiamen University, Xiamen 361005, China  
E-mail: yzyuan@xmu.edu.cn

[b] Prof. Dr. S. Li  
School of Chemical Engineering, Northwest University, Xi'an,  
Shaanxi, 710069, China

[c] Prof. Dr. X. Li  
School of Chemistry and Chemical Engineering, Pulp & Paper  
Engineering State Key Laboratory of China, South China University  
of Technology, Guangzhou 510640, China

Supporting information for this article is given via a link at the end of the document.



**Scheme 1.** Highly efficient HDO of lignin-derived oxygenates via the integration of active catalysts for C–O bond cleavage and aromatic hydrogenation.

catalysts for the efficient HDO of lignin-derived oxygenates and pyrolysis bio-oils (Scheme 1). The cleavage of inert  $C_{\text{aryl}}\text{OR}$  bonds to phenolics is mainly achieved on tungsten carbides ( $W_xC@CS$ , CS: carbon sphere), whereas aromatic rings are saturated by Ni catalysts, followed by a further aliphatic C–O bond cleavage of the resultant (alkyl)cyclohexanols on tungsten carbides or nickel catalysts. As a result, almost 100% of conversions of lignin-derived oxygenates with high efficiency can be achieved. High (alkyl)cyclohexanol or (alkyl)cyclohexane yields are obtained with different integrated manners of dual catalysts. The flexible use of integrated dual catalysts can catalyze the HDO of raw lignin bio-oils with almost-oxygen removal, reaching a total mass yield of up to 27.9% and carbon yield of up to 45.0%.

## Results and Discussion

The use of one bifunctional catalyst in the highly efficient multistep tandem reaction is challenging. For lignocellulose HDO, the critical difficulty originates from the competing ring saturation and C–O bond hydrogenolysis. We selected tungsten carbide as an active catalyst for C–O bond hydrogenolysis. Our previous works have found that optimized  $W_xC@CS$  with a preferable surface C/W atomic ratio of approximately 7–8 showed the best hydrogenolysis of guaiacol and other aromatic ethers to phenolics.<sup>[15]</sup> However, hydrogenation of phenolics, followed by further C–O bond cleavage, could not be achieved even when the reaction temperature was increased (Fig. 1, second column), thus leading to incomplete oxygen removal, which is always required for the utilization of ungradable bio-oils and complicated lignin-derived oxygenates. Our analysis clarified that further aromatic reduction is thermodynamically feasible for HDO reactions because a complete C–O bond cleavage is driven at low temperatures (Fig. S1). Nickel is a typical non-noble metal with excellent capability for  $H_2$  activation and constantly used in hydrogenation reactions.<sup>[9a–9c]</sup> Fig. 1 (first column) shows that the mono-Ni catalyst on carbon nanotubes (Ni/CNTs) is active for guaiacol HDO. However, the catalytic performance was

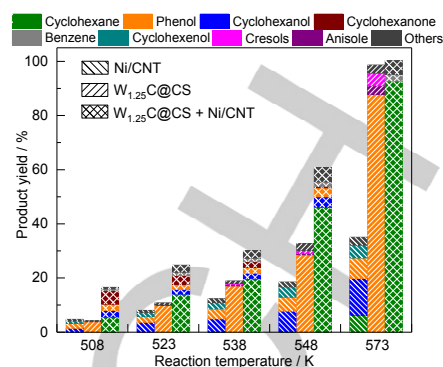


**Figure 1.** Catalytic performance of guaiacol HDO on several catalysts at different temperatures. Reaction conditions:  $P = 3.0$  MPa,  $H_2/\text{GUA}$  molar ratio = 50, liquid guaiacol flow =  $0.61 \text{ g h}^{-1}$ ; catalyst weight, 200 mg for  $W_xC@CS$  and 50 mg for Ni/CNT with 5.6 nm of Ni particle size,  $T = 508\text{--}573$  K.

unimpressive with poor selectivity, thereby indicating a competing aromatic reduction and C–O bond hydrogenolysis. Increasing the reaction temperature improved the product yield slightly. However, the presence of ring-saturated products, such as cyclohexanol, was still observed at low temperatures, thereby indicating that the Ni catalyst is a good candidate active for arene reduction.

The integration of these two components is expected to exhibit satisfied performance. The morphology of integrated dual catalysts shown in Fig. S2a demonstrated that Ni/CNTs were compacted on the outer surface of  $W_xC@CS$ .  $W_xC$  particles were well dispersed in the carbon spheres, whereas Ni particles were deposited on the CNTs from the EDX mapping and element analysis (Figs. S2e–S2f). The integration of dual catalysts showed no changes in active compositions, as observed in the XRD patterns (Fig. S3). Guaiacol HDO performance was remarkably enhanced by the combination of these two catalysts with increasing temperature and achieved almost oxygen removal with a cyclohexane up to 92.3% at 573 K as shown in Fig. 1. In fact, considerable efforts have been made to enhance the HDO performance by using Ni-based catalysts with optimized supports in previous reports.<sup>[16]</sup> For example, Bykova et al.<sup>[16a,b]</sup> used  $SiO_2\text{--}ZrO_2$  stabilized Ni and Ni–Cu catalysts (Ni: 37–58 wt.%) for HDO of guaiacol under 593 K with 17 MPa  $H_2$ , obtaining 63.9% yield of cyclohexane. Similar catalyst were reported by Zhang<sup>[16c,d]</sup> with a guaiacol conversion rate of  $6.8 \times 10^{-6} \text{ mol g}^{-1} \text{ s}^{-1}$  at 613 K. Zhao et al.<sup>[12a]</sup> employed 20 wt.% Ni/ZSM-5 for HDO of guaiacol at 523 K and 4 MPa  $H_2$ , achieving 100% conversion with 74% selectivity of cycloalkanes. Ni/ $SiO_2\text{--}Al_2O_3$  displayed a 45.0% yield of cyclohexane at 623 K.<sup>[16e]</sup> Thereby the integrated dual catalysts in our case showed superior performance compared with these results, which reveals the distinct advantage of separating C–O bond hydrogenolysis and arene reduction over two active catalysts.

Having identified the scope of the integrated dual catalysts for efficient HDO reactions, we also tested the HDO performance of various aromatics, such as veratrole and dimethoxyphenol, as shown in Table S1. Such compounds are typical in upgradable

lignin-derived oxygenates with high oxygen content. The cleavage of aryl C–O bond in the first step can be achieved by  $W_xC@CS$  (Table S2). In combination with the hydrogenation function in the Ni catalyst, almost-full conversion of substrates with nearly 100% deoxygenation could be obtained to produce oxygen-free hydrocarbons (mainly cyclohexane). Note, the optimized reaction temperatures were remarkably lower than the cases that used  $W_xC@CS$  alone. The overall yields ranged from 87.9% to 100.0% with a decreased temperature of 25–50 K. Clearly, the optimized reaction temperatures essentially maintained a highly efficient transformation with increased energy savings over the integrated dual catalyst.

To understand the roles of the two catalysts further, the product synthesis rate was investigated as a function of dual catalyst mass ratio (Fig. 2a). The use of Ni/CNT alone obtained a lower synthesis rate of eventual cyclohexane compared with that of intermediate phenol. This result confirmed incomplete deoxygenation and arene hydrogenation. The increase in the Ni/CNT/ $W_xC@CS$  mass ratio linearly increased the rates of phenol and cyclohexane formation in the initial stage. Interestingly, the slope of the increasing rate for cyclohexane was higher than that of phenol, thereby indicating the greater enhancement of further phenol transformation when the Ni catalyst was incorporated. For mass ratios greater than 0.125, the rates slowed down and generally reached the same constant ( $16.8 \times 10^{-6} \text{ mol s}^{-1} \text{ g}_{\text{cat}}^{-1}$ ) due to full intermediate phenolic conversion. Thus, the match activity for integrated dual catalysts is essential to achieve the best performance. To observe the roles of the two catalysts directly, we evaluated the conversions of intermediate phenol and cyclohexanol. Ni/CNT showed high activity of phenol hydrogenation, but cyclohexanol remained (Table S3). Deoxygenation of cyclohexanol was constantly achieved by using acid-catalyzed dehydration to form cycloalkane, followed by metal-catalyzed hydrogenation to cycloalkane.<sup>[12]</sup> By contrast, hydrogenolysis of cyclohexanol was easily achieved by  $W_xC@CS$  even though no activity was observed in phenol conversion. In our study, efficient C–O bond

cleavage and hydrogenation were mainly achieved with  $W_xC@CS$  and Ni/CNT, respectively. The two processes on the integrated dual catalysts drove each other to perform their adept functions as much as possible. Analysis of the Arrhenius plots derived the apparent activation energy ( $E_a$ ) shown in Fig. 2b to correlate the activities. The integration of dual catalysts displayed a considerably lower  $E_a$  at  $56.7 \text{ kJ mol}^{-1}$  compared with the single  $W_xC@CS$  and Ni catalyst. Chemisorption results (Table S4) showed enhanced  $H_2$  absorption with similar CO absorption over dual catalysts, thereby indicating that the Ni incorporation promoted hydrogen activation and aryl C–O bond cleavage over tungsten carbides. These results are corresponding to the interoperation of the dual catalysts.

The integration manner of different active catalysts was crucial in product selectivity (Fig. 3). The use of a dual-bed configuration with  $W_xC@CS$  downstream from Ni/CNT provided a wide product distribution (Fig. 3c). The formation of cyclohexane was due to the further C–O bond cleavage of cyclohexanol by downstream  $W_xC@CS$  based on the catalytic function of Ni/CNT. The increasing phenol selectivity suggested that certain remaining guaiacol were then transformed with tungsten carbides. The catalytic behavior changed when the streams of the two catalysts were reversed, as shown in Fig. 3d. High selectivity to cyclohexanol could be obtained with almost guaiacol conversion. No cyclohexenols were observed in this case, thereby suggesting that the responsibility of C–O bond hydrogenolysis over  $W_xC@CS$  contributed to the enhanced capability for arene reduction over Ni/CNT. Furthermore, the integration of dual catalysts with closed proximity remarkably improved the formation of cyclohexane and achieved high oxygen removal (Figs. 3e and 3f).

Motivated by the integration manners, we attempted to yield alternative chemicals directly in one reaction by tuning the active catalysts, which presumably provided the potential for the direct production of attractive chemicals from raw lignin-derived oxygenates. Previous reports have demonstrated that Ni is

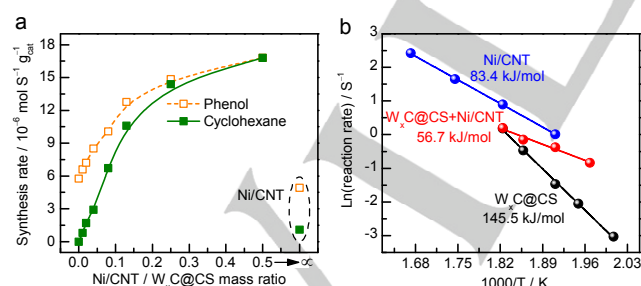


**Figure 2.** (a) Synthesis rate of the product in the guaiacol HDO of integrated dual catalysts with closed proximity as a function of the Ni/CNT/ $W_xC@CS$  mass ratio. Reaction conditions:  $P = 3.0 \text{ MPa}$ ,  $H_2/\text{GUA}$  molar ratio = 50, liquid guaiacol flow =  $1.22 \text{ g h}^{-1}$ , catalyst weight: 200 mg for  $W_xC@CS$  and 0–100 mg for Ni/CNT with 5.6 nm of Ni particle size,  $T = 573 \text{ K}$ . Note: The synthesis rate of phenol was calculated on the basis of the total products from phenol as an intermediate. (b) Arrhenius plots of the reaction rate  $\{\ln(r)\}$  versus  $1/T$  for guaiacol conversion over Ni/CNT (blue line),  $W_xC@CS$  (black line), and integrated dual catalysts (red lines).

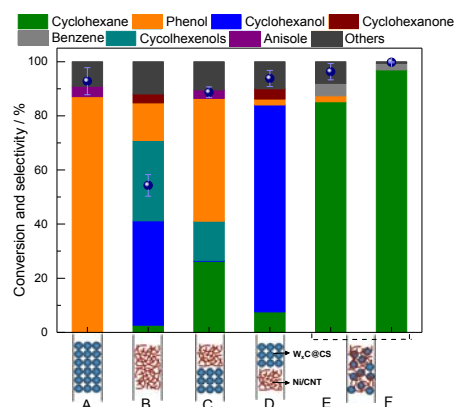


**Figure 3.** Effect of integration manner of different catalysts on the performance. (a)–(f) Using 200 mg for  $W_xC@CS$  and/or 50 mg for Ni/CNT; Ni particle size: (a)–(e) 20.5 nm and (f) 5.6 nm. Reaction conditions:  $P = 3.0 \text{ MPa}$ ,  $H_2/\text{GUA}$  molar ratio = 50, liquid guaiacol flow =  $0.61 \text{ g h}^{-1}$ ,  $T = 573 \text{ K}$ .

readily used for size control and displays structure sensitivity to HDO reaction.<sup>[9]</sup> Large particles were active for hydrogenation of the aromatic ring, whereas decreasing the particle size was preferable for deoxygenation. The Ni/CNT catalysts with different particle size distributions were successfully synthesized, as shown in Fig. S4a, and the particle sizes were determined using the TEM images and XRD patterns based on the Scherrer equation (Fig. S4b). These samples represented very different average particle sizes ranging from 5.0 nm to 20.0 nm. Further H<sub>2</sub>-TPR profiles (Fig. S5) revealed the reduction information of as-calcined Ni/CNT samples, implying that all Ni oxide species could be reduced based on our pretreatment procedure.<sup>[17]</sup> Fig. S6 shows the HDO performance of guaiacol over Ni/CNT catalysts. The conversion clearly decreased with the increase in particle size. The decreased cyclohexane selectivity suggested the suppression of deoxygenation capability, and only trace cyclohexane was formed in the case of large particles (20.5 nm). When W<sub>x</sub>C@CS was packed in the upper layer of Ni/CNT (Fig. 4a), guaiacol conversion clearly increased, and cyclohexanol selectivity was considerably enhanced with increasing Ni particle size. This finding was due to the role-sharing of the C–O bond cleavage on tungsten carbides that enabled Ni to perform optimized hydrogenation. The combination of upstream tungsten carbide and downstream Ni/CNT with large particles was preferable for the efficient production of cyclohexanol, which was also an important intermediate for the chemical production of cyclohexanone and adipic acid. The interoperation of dual catalysts was pronounced when they were mixed with closed proximity (Fig. 4b). Complete guaiacol conversion with 92.4%

cyclohexane selectivity was achieved when the Ni/CNT catalyst had a particle size of 5.6 nm. By further increasing the Ni particle size, conversions reduced slightly and cyclohexane selectivity remained high. Notably, the rapid conversion of intermediates on each catalyst remarkably enhanced HDO activity due to the thermodynamic driving force, which was confirmed when an aged W<sub>x</sub>C@CS with poor performance was used as one catalyst (Table S5). As shown in Scheme S1 for the possible reaction sequence, the enhanced performance was caused by the separated catalytic processes. Firstly, W<sub>x</sub>C@CS was mainly responsible for Ph–OCH<sub>3</sub> bond hydrogenolysis, followed by the hydrogenation of phenol to cyclohexanol over the Ni catalyst. Then the cleavage of the aliphatic C–O bond with hydrocarbon formation was readily achieved by W<sub>x</sub>C@CS or Ni particles. Given that the short catalyst lifetime is a common issue in HDO reactions, we also investigated the catalyst stability in guaiacol HDO under similar reaction conditions. Fig. 4c presents that the integrated dual catalysts (200 mg W<sub>x</sub>C@CS and 50 mg Ni/CNT(5.6 nm)) were stable in the HDO of guaiacol, and the deoxygenation efficiency remained unchanged after 150 h of reaction with the main product being cyclohexane. The structure of the used integrated dual catalysts composed of 200 mg W<sub>x</sub>C@CS and 50 mg Ni/CNT(5.6 nm) with a closed proximity was characterized by SEM, STEM, XRD and Ni particle estimation. The results are summarized in Fig. S7. As shown in Figs. S7a, a similar morphology of the integrated dual catalysts was observed by SEM. Further, insignificant changes of diffraction lines due to Ni species are shown for the used Ni/CNT (Fig. S7b), indicating the agglomeration of Ni nanoparticles might be limited after 150 h reaction. Nonetheless, STEM image in Fig. S7c revealed that a slight agglomeration of some Ni particles occurred after the reaction for 150 h. The estimation of Ni particle size distribution in Fig. S7d indicated that the average Ni particle size was slightly increased from 5.6 nm to 7.5 nm after run for 150 h. However, the integrated dual catalysts could keep at a high performance in terms of guaiacol conversion and cyclohexane selectivity even if the Ni particle size was larger than 10 nm as shown in Fig. 4b. The result is presumably due to the remarkable interoperation of dual catalysts. This finding shows a great potential of the integrated dual catalysts for practical applications.

On the basis of the above discussion, HDO of actual bio-oil was performed to determine the efficiency of integrated dual catalysts. The bio-oil from rapid pyrolysis was a brownish black liquid with 51.3 and 41.3 wt% carbon and oxygen content, respectively (Table S6). The compounds in the bio-oil were further identified via gas chromatography–mass spectrometry (GC–MS), as shown in Fig. S8a. Results showed that the bio-oil contained over 35 lignin-derived oxygenates, including acids, alcohols, furans, and mainly complex guaiacols (Fig. S8b). Table S7 lists the major groups of compounds involving simple oxygenates (e.g., acids, esters, alcohols, and ketones aldehydes), furans, and phenolics (e.g., phenols, guaiacols, syringols) at 35.4, 11.0, and 51.6 wt%, respectively. These

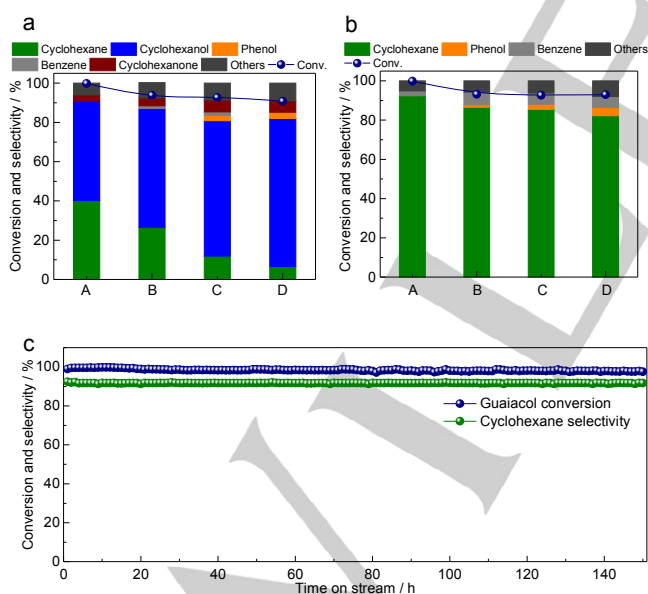


**Figure 4.** Catalytic performance for guaiacol HDO over (a) dual-bed configuration with Ni/CNT packed below W<sub>x</sub>C@CS and (b) integration of dual catalysts with closed proximity. The average Ni particle size in Ni/CNT catalyst: A. 5.6 nm, B. 10.2 nm, C. 13.5 nm, D. 20.5 nm. (c) Stability of integrated dual catalysts in the guaiacol HDO reaction. Reaction conditions: *P* = 3.0 MPa, H<sub>2</sub>/GUA molar ratio = 50, liquid guaiacol flow = 0.61 g h<sup>-1</sup>, catalyst weight = 200 mg for W<sub>x</sub>C@CS and 50 mg for Ni/CNT, and *T* = 573 K.

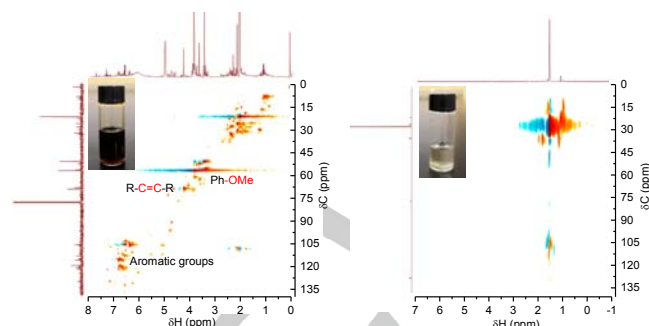
compounds were consistent with those reported in rapid pyrolysis.<sup>[18]</sup>

Table 1 compares the HDO performance of the actual bio-oil over different catalysts, and the results reveal that the major products were alkanes, cycloalkanes, alkylbenzenes, and alkylphenolics. The mono-Ni/CNT catalyst obtained a very low mass yield of total liquid alkanes (4.8 wt%) with certain alkylphenolics as products (Entry 1). By contrast,  $W_xC@CS$  showed nearly no activity for liquid (cyclo)alkane formation but obtained a 5.2 wt% mass yield of alkylphenolics (Entry 2). These compounds were mainly (alkyl)phenols as identified by GC–MS (Fig. S9). Results were consistent with the HDO products of lignin platform compounds over  $W_xC@CS$ . With the integration of a small amount of Ni/CNT and  $W_xC@CS$  under closed proximity (Entry 3), the mass yield of total liquid alkanes increased considerably and reached 13.6 wt%. Alkylphenolics were still observed in this case, and the mass yield increased to 7.0 wt%, although the Ni/CNT/ $W_xC@CS$  mass ratio was the same as those in HDO of simple lignin-derived compounds, as mentioned above. This finding was likely due to the insufficient hydrogenation function over the Ni/CNT catalyst in the HDO of the actual bio-oil. When more active Ni/CNT for hydrogenation was provided by further increasing the mass ratio (Entry 4), the total conversion of the actual bio-oil was obtained with a production of 27.9 wt% total liquid alkanes (Fig. S10). This result was significantly higher than that of Entry 3. The obtained alkanes included 0.2 wt% pentane, 0.9 wt% hexane, 9.9 wt% alkylcyclopentanes, and 16.5 wt% alkylcyclohexanes. The production of linear alkanes and alkylcyclopentanes suggested that HDO of furans and linear oxygenates from (hemi)cellulose was achieved. This finding was consistent with earlier reports. Overall, a 45 wt% of total carbon yield was obtained. Recently, Pt–Al<sub>2</sub>O<sub>3</sub>/HZSM-5 given a 77.27% conversion with 53.63% hydrocarbon selectivity in HDO of eugenol and exhibited activity in real bio-oil.<sup>[6b]</sup> A two-stage catalytic reactor was performed using Ru/C–Pt/ZrP for HDO of bio-oil, producing totally 30% carbon yield.<sup>[19]</sup> A significant contribution was achieved by Xia et

**Table 1.** HDO of actual bio-oil over mono Ni/CNT,  $W_xC@CS$ , and integrated dual catalysts with closed proximity.

Product	Mass yield <sup>a</sup> / carbon yield <sup>b</sup> (wt% / wt%)			
	Entry 1	Entry 2	Entry 3	Entry 4
Pentane	0.1 / 0.2	–	0.1 / 0.2	0.2 / 0.3
Hexane	0.3 / 0.5	–	0.4 / 0.8	0.9 / 1.4
Alkylcyclopentanes	1.2 / 1.8	–	5.9 / 9.5	9.9 / 15.9
Alkylcyclohexanes	2.3 / 3.5	–	7.2 / 10.8	16.5 / 26.7
Alkylbenzenes	0.2 / 0.3	0.1 / 0.2	0.1 / 0.2	0.4 / 0.7
Alkylphenolics	0.7 / 1.0	5.2 / 7.7	7.0 / 10.6	–
Total liquid alkanes	4.8 / 7.0	–	13.6 / 21.5	27.9 / 45.0

<sup>a</sup> Based on the mass of the actual bio-oil and <sup>b</sup> based on the mass of carbon in the actual bio-oil. Entry 1: 100 mg Ni/CNT, Entry 2: 200 mg  $W_xC@CS$ , Entry 3: integrated dual catalysts (200 mg for  $W_xC@CS$  and 50 mg for Ni/CNT), Entry 4: integrated dual catalysts (200 mg for  $W_xC@CS$  and 100 mg for Ni/CNT). Reaction conditions:  $P(H_2) = 3.0$  MPa,  $T = 598$  K,  $H_2$  flow = 125 mL/min, and liquid velocity = 0.008 mL/min.



**Figure 5.** 2D NMR spectra of the actual bio-oil (a) and obtained liquid products (b). The insets show the images of mixtures before and after HDO reaction.

al.<sup>[3c]</sup> that raw wood sawdust could be converted into liquid alkanes with 28.1% mass yield by using Pt/NbOPO<sub>4</sub> catalyst. Most alkanes were produced from (hemi)cellulose and the mass yield of (alkyl)cyclohexanes converted from lignin was only 5.1%. Further, Pd/m-MoO<sub>3</sub>–P<sub>2</sub>O<sub>5</sub>/SiO<sub>2</sub> was used in HDO of water-insoluble bio-oil, obtaining total liquid alkanes with 29.6% and 46.3% of mass and carbon yields, respectively.<sup>[11d]</sup> Therefore, our result is comparable to the investigations on catalytic performance over noble metal catalysts.

To demonstrate the clear advantage of the interoperation of integrated dual catalysts, we measured the 2D HSQC NMR spectra of the actual bio-oil and the obtained products (Fig. 5). The actual bio-oil displayed a wide distribution of compounds with typical aryl C–O bonds, C=C bonds, and aromatic functional groups (Fig. 5a). However, the obtained products showed centralized signals, which were assigned to the saturated C–H bond, thus revealing the almost-conversion of bio-oils into alkanes (Fig. 5b). The brownish black bio-oil became a transparent liquid after reaction, providing an additional evidence of the HDO efficiency (inset in Fig. 5). Specifically, oxygen content was reduced from 41.3 wt% of the bio-oil to 3.7 wt% of the obtained liquid (Table S6), indicating an almost-oxygen

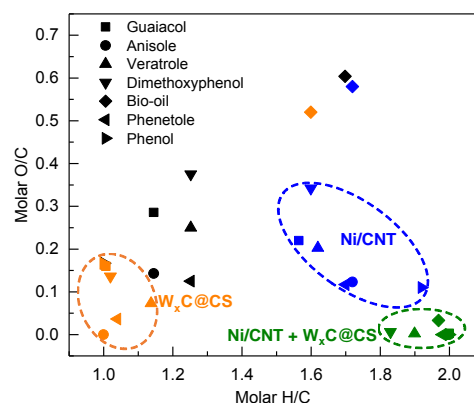


**Figure 6.** van Krevelen plot for the elemental compositions of raw reactants and the obtained products after HDO upgrading with various catalysts. The orange, blue and green points represent the compositions of products obtained via different catalysts.

removal. The H/C atomic ratio was approximately 1.97 which is closed to the atomic ratio of  $C_nH_{2n}$ , indicating the major products of cycloalkanes. It is worth noting that the compositions of liquid alkanes were similar to those of the conventional fuel oil shown in Table S6.<sup>[14,20]</sup> The van Krevelen plot was used to summarize the HDO efficiency of lignin-derived oxygenates and bio-oil in these catalysts (Fig. 6). A deep removal of oxygen content was achieved by using the integrated dual catalysts, whereas the use of mono Ni/CNT and  $W_xC@CS$  showed incomplete deoxygenation and hydrogenation. Therefore, the integrated dual catalysts achieved a remarkable interoperation of hydrogenation and C–O bond hydrogenolysis and possessed excellent catalytic performance for the simultaneous HDO of lignin-derived oxygenates and actual bio-oil into liquid alkanes.

## Conclusions

A catalytic strategy for the efficient HDO of lignin-derived oxygenates is successfully developed by separating the functions of C–O bond cleavage and aromatic hydrogenation on different active catalysts via interoperation. Tungsten carbide can effectively perform C–O bond hydrogenolysis, and Ni is mainly responsible for arene hydrogenation, followed by further C–O bond cleavage. Thus, almost 100% conversion of various oxygenates is obtained with decreasing reaction temperatures. Product distribution can be tuned by using the integration manners and active catalysts. High cyclohexane selectivity can be achieved by using the integrated dual catalysts with closed proximity (87.9%–100.0%). The control of the Ni particle size with downstream Ni/CNT plays a crucial role in the suppression of partial C–O bond cleavage that obtains high cyclohexanol selectivity. As for the actual pyrolysis bio-oil feedstock, the integrated dual catalysts show a state-of-the-art catalytic performance for the production of liquid alkanes with a total carbon yield of 45.0% and mass yield of 27.9%.

## Experimental Section

Tungsten carbide ( $W_xC@CS$ ) was prepared via careful carburization of hybrid organic–inorganic precursors in the presence of tungsten. The Ni/CNT catalysts were synthesized by controlling the heating ramp during the preparation. The integrated dual catalysts with closed proximity were prepared by physical grinding for 15 min. Conversions of lignin-derived oxygenates were performed using a fixed-bed reactor under different reaction conditions.

## Acknowledgements

This work was supported by the National Key Research and Development Program of China (2017YFA0206801), the National Natural Science Foundation of China (21972113 and 21473145), and the Program for Innovative Research Team in Chinese Universities (IRT\_14R31).

**Keywords:** Lignin-derived oxygenates • Hydrodeoxygenation • Dual catalysts • Tungsten carbides • Nickel catalysts

- [1] a) G. W. Huber, S. Iborra, A. Corma, *Chem. Rev.* **2006**, *106*, 4044; b) C. O. Tuck, E. Perez, I. T. Horvath, R. A. Sheldon, M. Poloakoff, *Science* **2012**, *337*, 695; c) C. Z. Li, X. C. Zhao, A. Q. Wang, G. W. Huber, T. Zhang, *Chem. Rev.* **2015**, *115*, 11559.
- [2] a) M. Zaheer, R. Kempe, *ACS Catal.* **2015**, *5*, 1675; b) M. V. Galkin, J. S. M. Samec, *ChemSusChem* **2016**, *9*, 1544.
- [3] a) H. M. Wang, J. Male, Y. Wang, *ACS Catal.* **2013**, *3*, 1047; b) B. E. Dale, R. G. Ong, *Biotechnol. Prog.* **2012**, *28*, 893; c) Q. N. Xia, Z. J. Chen, Y. Shao, X. Q. Gong, H. F. Wang, X. H. Liu, S. F. Parker, X. Han, S. H. Yang, Y. Q. Wang, *Nat. Commun.* **2016**, *7*, 11162; d) Z. W. Cao, J. Engelhardt, M. Dierks, M. T. Clough, G. H. Wang, E. Heracleous, A. Lappas, R. Rinaldi, F. Schuth, *Angew. Chem. Int. Ed.* **2017**, *56*, 2334.
- [4] S. Czernik, A. V. Bridgwater, *Energy Fuels* **2004**, *18*, 590.
- [5] a) D. Mohan, C. U. Pittman, P. H. Steele, *Energy Fuels* **2006**, *20*, 848; b) M. Saidi, F. Samimi, D. Karimpourfard, T. Nimmanwudipong, B. C. Gates, M. R. Rahimpour, *Energy Environ. Sci.* **2014**, *7*, 103.
- [6] a) J. Zakzeski, P. C. A. Bruijninx, A. L. Jongerius, B. M. Weckhuysen, *Chem. Rev.* **2010**, *110*, 3552; b) C. Ju, M. R. Li, Y. M. Fang, T. W. Tan, *Green Chem.* **2018**, *20*, 4492; c) G. H. Wang, Z. W. Cao, D. Gu, N. Pfander, A. C. Swertz, B. Spliethoff, H. J. Bongard, C. Weidenthaler, W. Schmidt, R. Rinaldi, F. Schuth, *Angew. Chem. Int. Ed.* **2016**, *55*, 8850; d) L. Offner-Marko, A. Bordet, G. Moos, S. Tricard, S. Rengshausen, B. Chaudrét, K. L. Luska, W. Leitner, *Angew. Chem. Int. Ed.* **2018**, *57*, 12721.
- [7] D. A. Ruddy, J. A. Schaidle, J. R. Ferrell III, J. Wang, L. Moens, J. E. Hensley, *Green Chem.* **2014**, *16*, 454.
- [8] a) J. Wildschut, F. H. Mahfud, R. H. Venderbosch, H. J. Heeres, *Ind. Eng. Chem. Res.* **2009**, *48*, 10324; b) T. Nimmanwudipong, C. Aydin, J. Lu, R. C. Runnebaum, K. C. Brodwater, N. D. Browning, D. E. Block, B. C. Gates, *Catal. Lett.* **2012**, *142*, 1190; c) Y. C. Lin, C. L. Li, H. P. Wan, H. T. Lee, C. F. Liu, *Energy Fuels* **2011**, *25*, 890.
- [9] a) J. He, C. Zhao and J. A. Lercher, *J. Am. Chem. Soc.*, **2012**, *134*, 20768; b) H. H. Fang, J. W. Zheng, X. L. Luo, J. M. Du, A. Roldan, S. Leoni and Y. Z. Yuan, *Appl. Catal., A: Gen.* **2017**, *529*, 20; c) A. R. Ardiyanti, S. A. Khromova, R. H. Venderbosch, V. A. Yakovlev, H. J. Heeres, *Appl. Catal. B Environ.* **2012**, *117–118*, 105; d) R. N. Olcese, M. Bettahar, D. Petitjean, B. Malaman, F. Giovanella, A. Dufour, *Appl. Catal. B Environ.* **2012**, *115–116*, 63; e) P. M. Mortensen, J. D. Grunwaldt, P. A. Jensen, A. D. Jensen, *Catal. Today* **2016**, *259*, 277.
- [10] a) W. Schutyser, S. V. d. Bosch, J. Dijkmans, S. Turner, M. Meledina, G. V. Tendeloo, D. P. Debecker, B. F. Sels, *ChemSusChem* **2015**, *8*, 1805; b) N. Yang, C. Zhao, P. J. Dyson, C. Wang, L. T. Liu, Y. Kou, *ChemSusChem* **2008**, *1*, 626.
- [11] a) Y. Yang, A. Gilbert, C. Xu, *Appl. Catal. A: Gen.* **2009**, *360*, 242; b) C. Zhao, Y. Kou, A. A. Lemonidou, X. B. Li, J. A. Lercher, *Angew. Chem. Int. Ed.* **2009**, *48*, 3987; c) K. L. Luska, P. Migowski, S. El Sayed, W. Leiner, *Angew. Chem. Int. Ed.* **2015**, *54*, 15750; d) H. H. Duan, J. C. Dong, X. R. Gu, Y. K. Peng, W. X. Chen, T. Issariyakul, W. K. Myers, M. J. Li, N. Yi, A. F. R. Kilpatrick, Y. Wang, X. S. Zheng, S. F. Ji, Q. Wang, J. T. Feng, D. L. Chen, Y. D. Li, J. C. Buffer, H. C. Liu, S. C. E. Tsang, D. O'Hare, *Nat. Commun.* **2017**, *8*, 591.
- [12] a) C. Zhao, J. A. Lercher, *Angew. Chem. Int. Ed.* **2012**, *51*, 5935; b) C. Zhao, J. He, A. A. Lemonidou, X. Li, J. A. Lercher, *J. Catal.* **2011**, *280*, 8; c) C. Zhao, J. A. Lercher, *ChemCatChem* **2012**, *4*, 64.
- [13] a) N. B. Van, D. Laurenti, P. Delichere, C. Geantet, *Appl. Catal. B: Environ.* **2011**, *101*, 246; b) X. Zhu, L. L. Lobban, R. G. Mallinson, D. E. Resasco, *J. Catal.* **2011**, *281*, 21; c) D. Y. Hong, S. J. Miller, P. K. Agrawal, C. W. Jones, *Chem. Commun.* **2010**, *46*, 1038; d) Q. N. Xia, Q. Cuan, X. H. Liu, X. Q. Gong, G. Z. Lu, Y. Q. Wang, *Angew. Chem. Int. Ed.* **2014**, *53*, 9755.
- [14] a) G. J. Wu, N. Zhang, W. L. Dai, N. J. Guan, L. D. Li, *ChemSusChem* **2018**, *11*, 2179; b) H. L. Wang, H. M. Wang, E. Kuhn, M. P. Tucker, B.

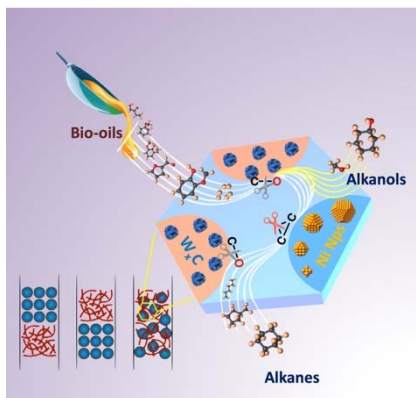
- Yang, *ChemSusChem* **2018**, *11*, 285; c) H. L. Wang, H. Ruan, M. Q. Feng, Y. L. Qin, H. Job, L. L. Luo, C. M. Wang, M. H. Engelhard, E. Kuhn, X. W. Chen, M. P. Tucker, B. Yang, *ChemSusChem* **2017**, *10*, 1846.
- [15] a) H. H. Fang, J. M. Du, C. C. Tian, J. W. Zheng, X. P. Duan, L. M. Ye, Y. Z. Yuan, *Chem. Commun.* **2017**, 53, 10295; b) H. H. Fang, A. Roldan, C. C. Tian, Y. P. Zheng, X. P. Duan, K. Chen, L. M. Ye, S. Leoni, Y. Z. Yuan, *J. Catal.* **2019**, 369, 283.
- [16] a) M. V. Bykova, D. Y. Ermakov, V. V. Kaichev, O. A. Bulavchenko, A. A. Saraev, M. Y. Lebedev, V. A. Yakovlev, *Appl. Catal. B: Environ.* **2012**, 113-114, 296; b) M. V. Bykova, D. Y. Ermakov, S. A. Khromova, A. A. Saraev, M. Y. Lebedev, V. A. Yakovlev, *Catal. Today* **2014**, 220-222, 21; c) X. H. Zhang, T. J. Wang, L. L. Ma, Q. Zhang, X. M. Huang, Y. X. Yu, *Appl. Energ.* **2013**, 112, 533; d) X. H. Zhang, T. J. Wang, L. L. Ma, Q. Zhang, Y. X. Yu, Q. Y. Liu, *Catal. Commun.* **2013**, 33, 15; e) H. Jahromi, F. A. Agblevor, *Appl. Catal., A: Gen.* **2018**, 558, 109.
- [17] a) A. B. Dongil, I. T. Ghampson, R. Garcia, J. L. G. Fierro and N. Escalona, *RSC Adv.* **2016**, 6, 2611; b) H. X. Yang, S. Q. Song, R. C. Rao, X. Z. Wang, Q. Yu, A. M. Zhang, *J. Mol. Catal. A Chem.* **2010** 1-2, 33; c) C. W. Hu, J. Yao, H. Q. Yang, Y. Chen, A. M. Tian, *J. Catal.* **1997**, 166, 1.
- [18] D. C. Elliott, T. R. Hart, G. G. Neuenschwander, L. J. Rotness, A. H. Zacher, *Environ. Prog. Sustain. Energy* **2009**, 28, 441.
- [19] K. Routray, K. J. Barnett, G. W. Huber, *Energy Technol.* **2017**, 5, 80.
- [20] E. Furimsky, *Appl. Catal. A: Gen.* **2000**, 199, 147.

Entry for the Table of Contents (Please choose one layout)

Layout 1:

## RESEARCH ARTICLE

Hydrodeoxygenation of lignin-derived oxygenates and the actual bio-oil can be effectively achieved via a tandem hydrogenolysis–hydrogenation strategy, whereas tungsten carbide is readily for C–O bond hydrogenolysis, and Ni is mainly responsible for arene hydrogenation. Product distribution can be tuned by the flexible use of integration manners and the active catalysts. A total mass and carbon yield to 27.9% and 45.0% is achieved by conversion of the actual bio-oil.



Huihuang Fang, Weikun Chen, Shuang Li, Xuehui Li, Xiping Duan, Linmin Ye, and Youzhu Yuan\*

Page No. – Page No.

**Tandem hydrogenolysis–hydrogenation of lignin-derived oxygenates over integrated dual catalysts with optimized interoperations**